Growth of Iron Oxide on Yttria-Stabilized Zirconia by Atomic Layer Deposition

Marco de Ridder, Patrick C. van de Ven, Rob G. van Welzenis, and Hidde H. Brongersma*

Faculty of Applied Physics, Eindhoven University of Technology, P.O. Box 513, 5600 MB Eindhoven, The Netherlands

Steve Helfensteyn and Claude Creemers

Fysico-Chemistry Laboratory, Catholic University Leuven, W. de Croylaan 46, B-3001 Leuven, Belgium

Pascal Van Der Voort, Michael Baltes, Mariska Mathieu, and Etienne F. Vansant

Laboratory of Adsorption and Catalysis, Department of Chemistry, University of Antwerp (UIA), Universiteitsplein 1, B-2610 Wilrijk, Belgium

Received: May 9, 2002

The growth and thermal stability of an iron oxide overlayer on yttria-stabilized zirconia (YSZ) have been studied using atomic layer deposition (ALD), mainly in combination with low-energy ion scattering (LEIS). These techniques form a powerful combination, where ALD is designed for controlled (sub)monolayer deposition, while LEIS selectively probes the altered outermost atomic layer. The $Fe(acac)_3$ precursor reacts already at room temperature with YSZ. The reaction proceeds until saturation, which is characteristic for ALD. After the results of repeated ALD cycles, which consist of $Fe(acac)_3$ deposition followed by an oxidation treatment, have been studied, a model could be proposed which describes the growth mode of the iron oxide layer on YSZ. Oxidation at temperatures of 800 °C and higher causes a migration of Fe_2O_3 into the bulk, limiting its usefulness in surface catalytic processes at these temperatures. At 800 °C the diffusion coefficient of Fe in YSZ is determined to be 10^{-23} m^2/s. The reaction mechanism of $Fe(acac)_3$ with the YSZ surface is studied using infrared diffuse reflectance. The results reveal more than one reaction mechanism, but there seems to be a preference for the reaction via coordinatively unsaturated sites.

1. Introduction

Atomic layer deposition (ALD), also known as atomic layer epitaxy (ALE), is a controlled layer-by-layer deposition technique.[1−5] The deposition is self-controlled through saturating reactions between the surface and the reactants. The saturation is only achieved under certain reaction conditions, which depend mainly on the surface temperature of the substrate in combination with the reactants.

ALD is well suited for growing uniform compound layers on both flat substrates[1,2] and porous, heterogeneous oxidic surfaces.[4,6] In this study we used ALD to modify the yttria-stabilized zirconia (YSZ) surface using iron acetylacetonate ($Fe(acac)_3$) and oxygen as precursors. YSZ is an ionic conductor often used in solid oxide fuel cell (SOFC) technology. The surface oxygen exchange at the YSZ surface is the bottleneck in the performance of the SOFC.[7−9] Improvement of the surface oxygen exchange reaction seems to be achieved by modification of the surface by, e.g., ion implantation[10,11] or thin film deposition. Iron is a likely candidate for the improvement of the surface oxygen kinetics. It has multiple valences needed for the conversion of gaseous oxygen molecules to oxide ions that can diffuse through the solid electrolyte. Moreover, Sasaki and Maier[12] showed that, while Fe mainly has the 3+ valence under the highly oxidizing conditions of the SOFC (1000 °C, 1 bar of O_2), about 0.6% Fe is present in the 2+ valence state.

Reaction of metal acetylacetonate with an oxidic surface generally proceeds via surface hydroxyl groups.[13,14] $Fe(acac)_3$ has three acetylacetonate ($C_5H_7O_2$) (acac) ligands in octahedral arrangement.[15−17] The steric hindrance of three acac ligands prevents close approach of surface OH groups to the central Fe ion in the complex. Therefore, $Fe(acac)_3$ has to lose one or more ligands before it can react with the surface. Loss of acetonate ligands is reported by Kenvin et al.[18] and Van Ommen et al.[19] Kenvin et al. reported the loss of one acac ligand by $Fe(acac)_3$ in the reaction with silica surfaces. Van Ommen et al. investigated the adsorption of $Fe(acac)_3$ on TiO_2. Two acac ligands are lost in this reaction in the form of acetylacetone (Hacac). By continuous adsorption of $Fe(acac)_3$ an almost complete monolayer of Fe_2O_3 could be achieved on TiO_2. Kenvin et al. and Van Ommen et al. used liquid impregnation at room temperature (RT) for their experiments, which is quite different from ALD. However, the reaction at RT did show the instability of the $Fe(acac)_3$ complex, for which steric hindrance and the activation energy needed for chemisorption are easily overcome.

Here, we present a study on the reaction of $Fe(acac)_3$ with the YSZ surface, where the focus will be on the growth and thermal stability of the created iron oxide layer on the YSZ surface. The combination of low-energy ion scattering (LEIS) and ALD has proven to be very fruitful for such a purpose.[6,20] ALD provides the ability to produce the desired surface modifications, while the atomic composition of the outermost

* To whom correspondence should be addressed. Phone: +31 40 247 4281. Fax: +31 40 245 3587. E-mail: H.H.Brongersma@tue.nl.

10.1021/jp0211640 CCC: $22.00
Published on Web 12/03/2002

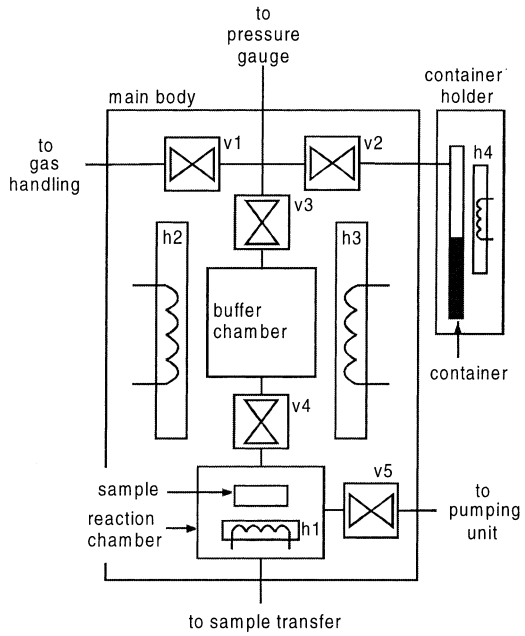

Figure 1. Schematic of the growth chamber of the ALD setup. Valves are indicated by v1−v5, and heaters are indicated by h1−h4. The main body and container holder are situated in a stainless steel vessel with a standard pressure in the low 10^{-7} mbar range. Gas (N_2, O_2) from the gas handling is let into the main body via a flow controller. The sample transfer is connected to the pretreatment chamber of the LEIS setup.

surface of highly dispersed insulating substrates can be quantified with LEIS.

2. Experimental Section

2.1. ALD Setup. The growth experiments are performed in an improved version of the ALD apparatus, as described in detail in ref 21. A schematic of the newly designed growth chamber is given in Figure 1. The sample is placed in the reaction chamber, which has a volume of about 1 cm^3 and is similar to that in the former design. The precursor ($Fe(acac)_3$) is valved into the reaction chamber using its own vapor pressure (no carrier gas is used). Inlet of purge gas (N_2) and oxidant gas (O_2) is controlled via a flow controller. The chamber surrounding the main body and container (not depicted in Figure 1) can be pumped down to a pressure of 10^{-7} mbar. This minimizes heat loss to the surroundings, but also prevents unwanted gas particles from leaking into the reaction chamber. The buffer chamber gives control over the amount of precursor used in the reaction. This is especially useful for studying ALD reactions in the presaturation regime. The buffer has a volume of approximately 1 cm^3. It can be heated to 500 °C. The heater, like all other heaters in the ALD setup, is controlled by a PID controller (WEST 9100). The temperature is monitored by thermocouples. Temperature stability is obtained within 1 °C. At present, the valves in the main body (indicated by v1−v5 in Figure 1) are made of a synthetic material, which does not withstand temperatures in excess of 200 °C. As the ALD experiments have to be performed below the decomposition temperature of $Fe(acac)_3$, which is 180 °C in the absence of O_2,[22] the restriction of the maximum allowable temperature for heaters h2 and h3 does not impose a problem. The container that holds the $Fe(acac)_3$ has a volume of about 2 cm^3. It is easily removable from its holder to refill or change the precursor. Besides heating the container to 500 °C, it can also be cooled to −70 °C using liquid nitrogen.

2.2. Measurements. *2.2.1. Sample Preparation.* The following samples are used: 8 mol % Y_2O_3 doped ZrO_2 (8YSZ), 10 mol % Y_2O_3 doped ZrO_2 (10YSZ), α- Fe_2O_3, and γ-Fe_2O_3.

LEIS measurements are done on 10YSZ, α- Fe_2O_3, and γ-Fe_2O_3. The 10YSZ samples are made from powder supplied by Tosoh Co., Japan (Al_2O_3, <0.005 wt %; SiO_2, <0.002 wt %; Fe_2O_3, <0.002 wt %; Na_2O, ∼0.001 wt %). The powder, mixed with 5 wt % paraffin as a binder, is first pressed uniaxially and then isostatically (100 MPa) into disks 10 mm in diameter and 1.5 mm thick. Sintering is carried out at 1400 °C in ambient air for 2 h in a tube furnace, after the added paraffin is removed by slow heating at temperatures below 600 °C. The preparation of γ-Fe_2O_3 has been described in ref 23, while α-Fe_2O_3 is obtained from Merck, Germany. The bulk structure of these oxidic powders is verified with X-ray diffraction. After introduction of a sample in the pretreatment chamber of the LEIS setup, the sample surface is cleaned. The cleaning procedure consists of a high-vacuum ($<1 \times 10^{-6}$ mbar) anneal at 300 °C for 2 min, followed by an oxidation treatment with atomic oxygen for 10 min at 10^{-4} mbar (the microwave input power of the oxygen atom source is 150 W).[24] This procedure results in a surface free of water and organic contaminants. Subsequently, the 10YSZ samples are sputtered with 1 keV $^{40}Ar^+$ ions (maximum dose 1×10^{15} ions/cm^2) to remove impurities (SiO_2, CaO, Na_2O) which have segregated from the bulk to the surface during manufacturing. To restore the stoichiometry, the samples are oxidized using the atomic oxygen source (10 min, 10^{-4} mbar of O_2, 150 W). After all these treatments the LEIS spectra of the 10YSZ samples only show oxygen and yttrium/zirconium peaks.

ALD cycles are only performed on the 10YSZ samples. The sample is placed in the reaction chamber, and the sample, container, and main body are heated to the desired temperatures T_s, T_c, and T_m, respectively. After temperature stabilization, $Fe(acac)_3$, obtained from Acros Organics, Belgium, is admitted to the buffer chamber. Next, the valves between the buffer chamber and container are closed, and the valve between the buffer chamber and reaction chamber is opened for a fixed time interval (t_e). Hereafter, the redundant $Fe(acac)_3$ is removed by flushing with N_2 for 5 min. The last step is the removal of the organic ligands by means of oxidation. This is done in the reaction chamber by thermal oxidation up to 300 °C (O_2 flow) or in the pretreatment chamber by thermal oxidation up to 500 °C (O_2 refreshed every 5 min) or by atomic oxidation (see the cleaning method).

After 10 ALD cycles, several 10YSZ samples are oxidized in a conventional tube oven at 800 and 1000 °C for 5 h in an O_2 flow for studying the thermal stability of the deposited iron oxide layer.

X-ray photoelectron spectroscopy (XPS) measurements are performed on a 10YSZ sample after one ALD cycle. Diffuse reflectance infrared Fourier transform (DRIFT) measurements are done on 8YSZ (TOSOH Co., 8 m^2/g) and α-Fe_2O_3. $Fe(acac)_3$ is adsorbed on the sample surfaces by means of a liquid-phase reaction.[25,26] Both support materials (8YSZ and α-Fe_2O_3) are dried in air for 16 h at 400 °C. Toluene solutions (about 50 mL) with 2 g of support (8YSZ or α-Fe_2O_3) and 0.5 g of $Fe(acac)_3$ are stirred for 2 h at 80 °C. Hereafter, the reacted powders are washed 3−5 times with 50 mL of toluene at 50 °C and dried at 80 °C in a vacuum.

2.2.2. Analysis. The LEIS measurements are performed at RT on the setup called NODUS[27,28] using a 3 keV $^4He^+$ incident ion beam. An ion dose of about 1×10^{14} ions/cm^2 is needed to measure one LEIS spectrum. To prevent the samples from

TABLE 1: Fractional Surface Fe_2O_3 Coverage on 10YSZ Obtained after One ALD Cycle Performed under Standard and Other Experimental Conditions[a]

settings	fractional Fe_2O_3 coverage	settings	fractional Fe_2O_3 coverage	settings	fractional Fe_2O_3 coverage
standard	0.08 ± 0.03	$T_s = 90$ °C	0.08 ± 0.03	$t_e = 2$ days	0.09 ± 0.02
$T_c = 40$ °C	0.09 ± 0.03	$T_s = 150$ °C	0.09 ± 0.01	no flushing	0.08 ± 0.03
$T_c = 60$ °C	0.07 ± 0.03	$t_e = 10$ min	0.07 ± 0.02		

[a] Standard conditions are $T_c = T_m = T_s =$ RT, $t_e = 2$ min, flushing with N_2 for 5 min, and atomic oxidation. For the other experiments, only the settings different from the standard are indicated.

becoming charged, their surfaces are flooded with low-energy electrons. The Y and Zr peaks cannot be separated in the LEIS spectra, because the mass difference between Y and Zr is too small. The observed peak is, therefore, referred to as the (Y, Zr) peak.

The XPS measurements are performed on the setup called ERISS. The Mg Kα radiation (1253.6 eV) is produced by a dual-anode X-ray source from VG (type XR3E2). The analyzer is a double-toroidal electrostatic analyzer.[29] The DRIFT measurements are performed on a Nicolet Nexus 670 bench.[30]

3. Results and Discussion

3.1. ALD of Iron Oxide on 10YSZ. The deposition of Fe(acac)$_3$ on 10YSZ is performed under various experimental conditions, but each time starting from a clean, Fe-free, 10YSZ surface. The results of these experiments are summarized in Table 1. Standard conditions for an ALD experiment are a container, a main body, a sample temperature (T_c, T_m, T_s) of 25 °C (RT), an exposure time (t_e) of the sample to Fe(acac)$_3$ of 2 min, flushing with N_2 for 5 min, and oxidation using atomic oxygen. Under these standard conditions, 8(±3)% of the initial 10YSZ surface is covered by Fe_2O_3 after the ALD experiment. This value is in agreement with sterical hindrance effects limiting further reaction (see section 3.3.1). The conversion of the Fe LEIS signal to an Fe_2O_3 coverage is described in section 3.2.1. The gas-phase reaction of Fe(acac)$_3$ with 10YSZ is a surface-saturating reaction, which is confirmed by experiments with longer reaction times and higher Fe(acac)$_3$ vapor pressures. The surface Fe_2O_3 coverage does not increase when the reaction time is increased from 2 min to 2 days (the connection between the container and reaction chamber is open during the 2 days), nor does it change when the container temperature is raised from 25 to 60 °C (see Table 1).

The substrate surface temperature is an important variable in the ALD process. The temperature should be high enough to overcome the activation energy needed for chemical bonding and to prevent multilayer condensation. However, the temperature should not be so high that it causes reevaporation of the reactants from the surface. The temperature window in which the ALD process takes place is often fairly wide. This means that accurate temperature control is not necessary. Changing the substrate temperature from RT to 150 °C results (within experimental error) in the same Fe_2O_3 surface coverages (see Table 1), which makes the temperature window at least 125 °C wide.

Flushing removes gas-phase Fe(acac)$_3$. Since the Fe_2O_3 coverage does not change when the flushing step is omitted (see Table 1), Fe(acac)$_3$ does not adsorb significantly on Fe(acac)$_3$.

The oxidation step is necessary to remove the organic ligands from the surface. From an earlier study we know that it is difficult to remove hydrocarbons from the 10YSZ surface.[24] Therefore, different oxidation treatments have been tried. Typical LEIS spectra recorded after one ALD cycle, using different oxidation treatments, are given in Figure 2. Thermal oxidation treatments at temperatures between 150 and 500 °C in 2−200 mbar of O_2 for 5−30 min do not result in the complete removal of the organic ligands, as can be concluded from the low intensity and the missing surface peaks in the LEIS spectra (spectra a and b in Figure 2). Higher oxidation temperatures cannot be used in our setup, but would also cause Fe_2O_3 to migrate into the bulk (see section 3.4). The results seem to be in contrast with findings reported in the literature, where adsorbed acac ligands are readily removed by oxidation to 300 °C in air.[30] The acetylacetonate is converted to acetate with the release of acetone at 110 °C. Water is needed for this reaction. The remaining acetate group is removed by oxidation at 300 °C. In our case, the low intensity and the absence of surface peaks in the LEIS spectra might be attributed to cross-contamination from chamber walls or the adsorption of reaction products. Atomic oxygen is much more reactive than molecular oxygen. Using this treatment, the ligands are removed completely (spectrum c in Figure 2). Clear O, Fe, and (Y, Zr) peaks are visible in the LEIS spectra. Repeating the atomic oxidation does not change the spectrum any further.

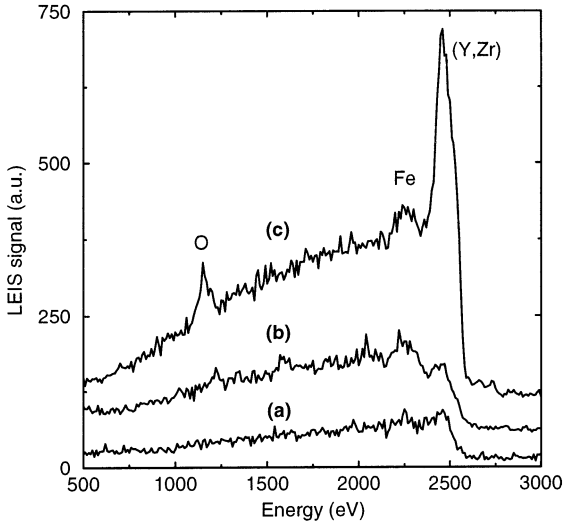

Figure 2. LEIS spectra (3 keV, $^4He^+$) after one ALD cycle, using different oxidation treatments. The oxidation treatments used are (a) thermal oxidation at 150 °C in 2 mbar of O_2 flow for 5 min, (b) thermal oxidation at 500 °C in 2 mbar of O_2 for 30 min (O_2 is refreshed every 5 min), and (c) atomic oxidation (RT, 10^{-4} mbar, 10 min, 150 W). Spectra are shifted vertically for clarity. Without the shift the background signals at energies above 2600 eV are equal.

The oxidation state of Fe after the complete ALD cycle is determined with XPS. The binding energy of the Fe $2p_{3/2}$ peak is determined to be 710.7 ± 0.6 eV. This value is in good agreement with Fe being present as Fe_2O_3. However, due to the uncertainty in the binding energies,[31] it cannot be excluded whether a small fraction of the Fe is still present as FeO or Fe_3O_4.

3.2. Multicycle Growth. *3.2.1. Increasing Fe_2O_3 Coverage.* The growth of Fe_2O_3 on the 10YSZ surface can be controlled

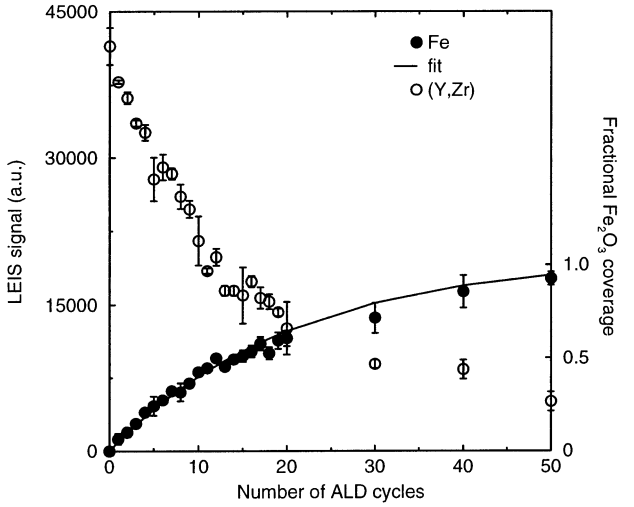

Figure 3. Fe and (Y, Zr) LEIS signals for ALD cycle numbers 0−50. LEIS spectra are measured with a 3 keV $^4He^+$ incident ion beam. Each LEIS measurement is done directly after the ALD cycle. The Fe signals are indicated by the filled circles, the (Y, Zr) signals by the open circles. The solid curve indicates the increase of the Fe signal with ALD cycle number, if it is assumed that 5% of the free YSZ surface is covered after each ALD cycle. The right *y*-axis labels are the result of the conversion of the Fe LEIS signals to Fe_2O_3 surface coverages.

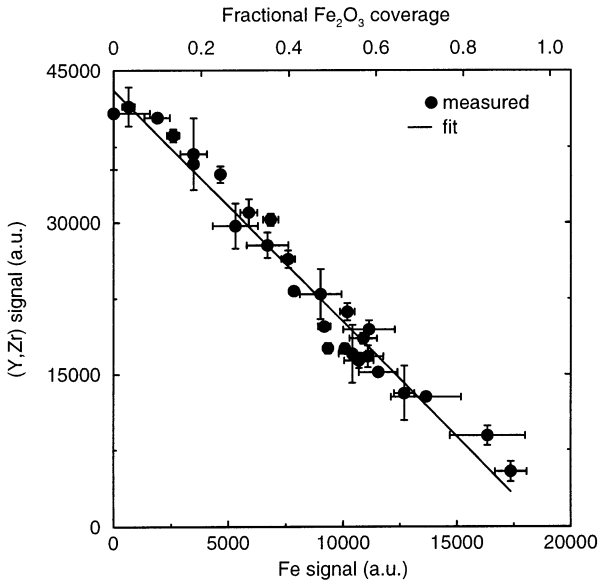

Figure 4. Fe signal versus (Y, Zr) signal. Signals are taken from Figure 3. Maximum Fe signal (the (Y, Zr) signal is zero) agrees with full coverage by Fe_2O_3. The maximum (Y, Zr) signal (the Fe signal is zero) agrees with a completely uncovered YSZ surface. The fit is based on the least-squares method.

by the number of ALD cycles. The Fe_2O_3 coverage, which is the part of the YSZ surface that is covered by Fe_2O_3 irrespective of the thickness of the Fe_2O_3 layer, is determined after 0−50 ALD cycles. Each measurement is done on a new sample position to avoid changes induced by sputtering. The ALD experiments are performed under the following conditions: $T_s = T_m = T_c =$ RT, $t_e = 5$ min, no flushing, and atomic oxidation. The results of the increase in the Fe signal and decrease in the (Y, Zr) signal as a function of the number of ALD cycles are shown in Figure 3. After 50 cycles the Fe_2O_3 still does not cover the 10YSZ surface completely. The O yield (not shown) remains constant for all cycle numbers.

Conversion of the LEIS signals to surface coverages is deduced from the relation between the increasing Fe signal and the decreasing (Y, Zr) signal (Figure 4). Strictly speaking, the system should be considered a four-component system (O, Fe, Y, and Zr). Treatment as a two-component system (Fe_2O_3, 10YSZ) is reasonably justified as the intensity of the O signal is independent of the surface composition. A linear relation between the increasing LEIS signals of Fe and the decreasing LEIS signals of (Y, Zr) is found. The maximum Fe signal, which agrees with a (Y, Zr) signal of zero, corresponds with an Fe_2O_3 coverage of one and is found after extrapolation. The Fe LEIS signals can now be converted to Fe_2O_3 coverages. The result is indicated in Figure 3 by the right *y*-axis labels.

Because of the stepwise increase of the Fe_2O_3 coverage, the following relation between the number of ALD cycles (n) and the Fe_2O_3 coverage ($\theta(Fe_2O_3)$) is found and is indicated by the solid curve in Figure 3:

$$\theta(Fe_2O_3) = 1 - \left(1 - \frac{1}{20 \pm 2}\right)^n = 1 - 0.95^n \qquad (1)$$

This means that, on average, 5.0(±0.5)% of the free YSZ surface is covered by Fe_2O_3 after each ALD cycle. This value is somewhat lower than the 8(±3)% coverage after the first ALD cycle (section 3.1), but agrees within the accuracy with which the low Fe_2O_3 coverage can be determined.

3.2.2. Sputter Profiles. The results of the Fe and (Y, Zr) sputter profiles are shown in Figure 5. The Fe signal first increases to a maximum, but then decreases with sputter dose. The (Y, Zr) signal increases with sputter dose until the maximum value is reached. The O signal (not shown) remains constant for all sputter doses and all initial Fe_2O_3 coverages.

The sputter profiles clearly show that the deposition of Fe_2O_3 is not restricted to one monolayer. The sputter dose needed for the (Y, Zr) signal to reach its maximum value (and for the Fe_2O_3 to be removed completely) increases with the number of ALD cycles. The (Y, Zr) signals are (at least) 90% of their maximum values after using sputter doses of 6×10^{15}, 27×10^{15}, and 68×10^{15} $^4He^+$ ions/cm^2 for, respectively, 3, 20, and 50 ALD cycles. Assuming sputter yields for Fe, Y, and Zr of about 0.1 for sputtering with 3 keV $^4He^+$ ions[32,33] and knowing that the sputter yields of oxides are in general lower than those of metals,[34] maximum thicknesses of the Fe_2O_3 layers are estimated at, respectively, about one, three, and seven layers (the atomic surface density is about 10^{15} particles/cm^2).

The increase of the Fe signal with sputter dose observed in Figure 5a can be explained by preferential removal of the oxygen and/or by a change in structure. Preferential sputtering of O on Fe_2O_3 has been reported for sputtering with $^{40}Ar^+$ and $^{131}Xe^+$ ions.[35,36] Similar effects can be expected for sputtering with $^4He^+$ ions on Fe_2O_3. Structural changes occur when Fe_2O_3 transforms into Fe_3O_4 or when γ-Fe_2O_3 transforms into α-Fe_2O_3. The preferential removal of oxygen might invoke the (local) structural change from Fe_2O_3 to Fe_3O_4. From exposure of metallic Fe to O_2 we know that Fe_3O_4 is formed before Fe_2O_3 and that upon sputtering with $^4He^+$ ions the reverse process occurs. LEIS spectra of α- and γ- Fe_2O_3 (Figure 6) show that the Fe signal of γ-Fe_2O_3 is only 78(±5)% of that of α-Fe_2O_3, which agrees with earlier results.[37] The spectra are scaled with respect to the O signal. The difference can be explained on the basis of their atomic structures. The corundum structure of α-Fe_2O_3 consists of a hexagonal close packing of oxygen ions with the Fe ions in the octahedral interstitial sites.[38] Since there are equal amounts of O ions and octahedral interstices, only two-thirds of the available interstitial sites are occupied. The predominant surface plane is the (0001) face with 8 Fe ions for every 12 O ions. Using the result of Figure 6, only 6 Fe ions

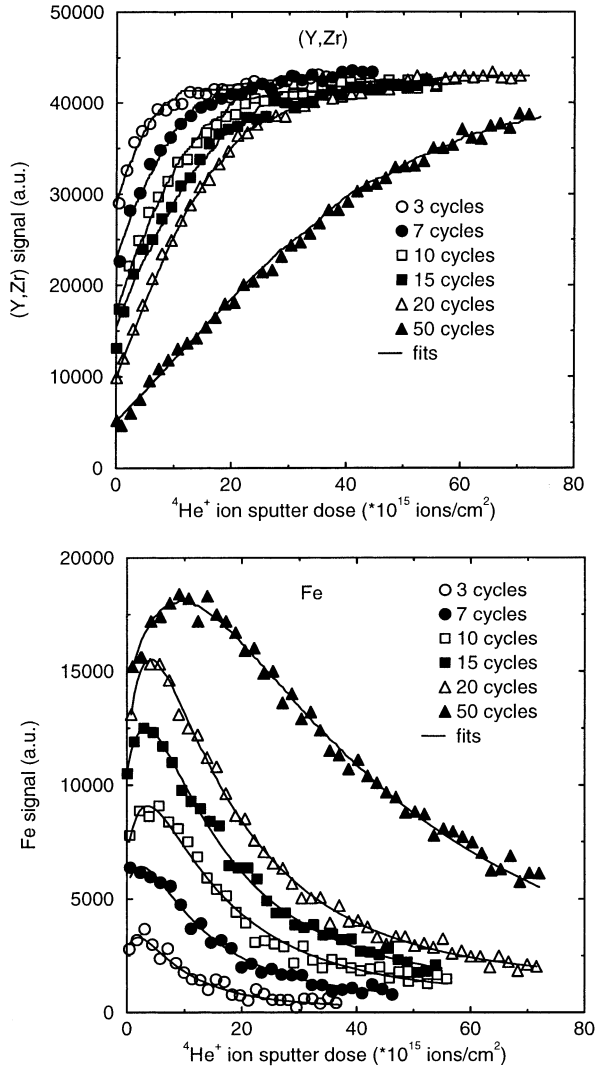

Figure 5. Sputter profiles of Fe and (Y, Zr) measured with 3 keV $^4He^+$ ions after 3, 7, 10, 15, 20, and 50 ALD cycles. ALD cycle conditions are $T_c = T_m = T_s = RT$, $t_e = 5$ min, no flushing, and atomic oxidation. (a, top) shows the Fe signal versus the sputter dose. (b, bottom) shows the (Y, Zr) signal versus the sputter dose. Simulations of the sputter profiles are given by the solid curves. They are based on a random sputter model, which is described in section 3.2.3.

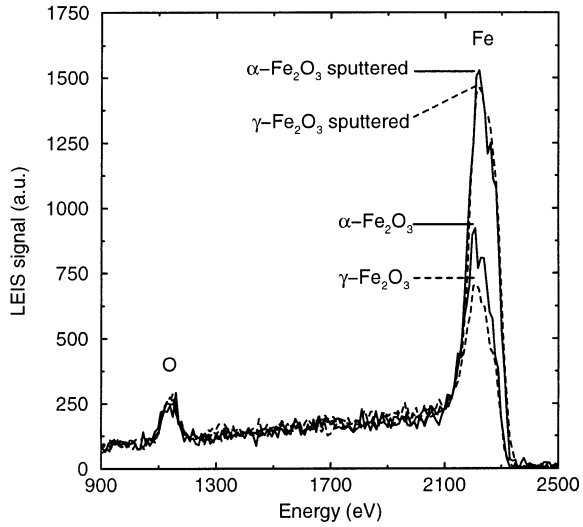

Figure 6. LEIS spectra (3 keV $^4He^+$) of α-Fe_2O_3 and γ-Fe_2O_3. LEIS spectra are normalized with respect to the O signal. For both oxides a spectrum is given, which is measured directly after surface cleaning and after prolonged sputtering (sputter dose of 6×10^{16} $^4He^+$ ions/cm^2).

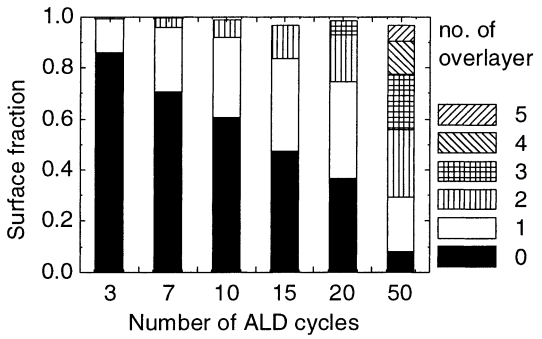

Figure 7. Surface configuration after 3, 7, 10, 15, 20, and 50 ALD cycles. For each surface the fractions of uncovered (black boxes) and covered YSZ are indicated. The arrangement of deposited Fe_2O_3 is also given (only for fractions larger than 5%). The arrangement is based on a random sputter model.

for every 12 O ions are visible in the case of γ-Fe_2O_3. γ-Fe_2O_3 has a (defective) spinel structure. For spinel surfaces it is known that only the octahedral cation sites are visible for LEIS.[39] From the low index planes which are usually considered as surface planes[40] only the B(111) and D(110) surface planes comply with this restriction. With the additional restriction of the anion/cation ratio of 2, this leads to the D(110) surface plane, which is in agreement with results found for Al_2O_3.[41] Upon sputtering the Fe signal increases and the O signal decreases for both α- and γ-Fe_2O_3, resulting in equal Fe/O ratios for both oxides, which is expected on the basis of their bulk stoichiometries. The LEIS spectra of α- and γ-Fe_2O_3 after prolonged sputtering (dose of 6×10^{16} $^4He^+$ ions/cm^2) are also given in Figure 6.

3.2.3. Modeling Growth and Sputter Profiles. On the basis of the results of the multicycle growth, it is assumed that random deposition of $Fe(acac)_3$ results in a 5% coverage of the surface with Fe_2O_3 after each ALD cycle. No distinction is made between deposition of $Fe(acac)_3$ on YSZ or on Fe_2O_3 that has been deposited in previous ALD cycles. Because of the low deposition temperature, the mobility of the Fe species will be negligible. The Fe_2O_3 growth on the sample can now be calculated and is given in Figure 7. The fraction of the uncovered 10YSZ surface decreases while the fraction of the 10YSZ surface covered by Fe_2O_3 increases in accordance with the results of Figure 3. The growth process does not cause a layer-by-layer growth, but a pyramid-like growth, which means part of the 10YSZ surface is covered by one overlayer of Fe_2O_3, part by two overlayers of Fe_2O_3, etc. This arrangement is also given in Figure 7.

To verify the assumption made in the growth model, the sputter profiles of Figure 5 are simulated using a random sputter model. In this model the sample is represented by a one-dimensional surface consisting of 100 atoms. The sample thickness equals 25 atomic layers. This is more than sufficient to reach a steady state, which means the sputter profile does not change anymore upon further sputtering. The atoms are sputtered randomly. The sputter yields for all atoms are taken equal and constant. The results of the model calculations of the (Y, Zr) sputter profiles are included in Figure 5b. Good agreement between the profiles and model is obtained. It must be noted that the YSZ surface is oxygen terminated, which causes a deviation between simulated and measured sputter profiles at doses lower than 10×10^{15} ions/cm^2. The fits are corrected for this effect by taking into account that part of the (Y, Zr) is initially covered by oxygen. Simulations of the Fe sputter profiles are more complicated than those of the (Y, Zr)

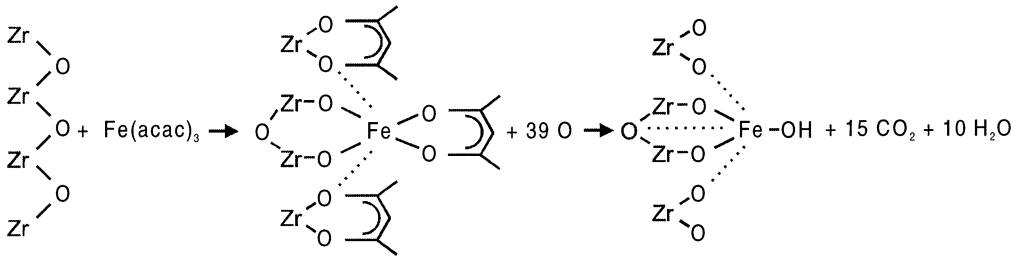

Figure 8. Reaction mechanism of $Fe(acac)_3$ with the YSZ surface. Fe strives for a 6-fold coordination with surrounding oxygen ions. The dashed lines indicate the additional coordination of the central Fe ion with oxygen ions. The actual bond angles might look distorted in the two-dimensional representation.

sputter profiles due to the (structural) changes at low sputter doses. Agreement between simulations and measured Fe sputter profiles is obtained when it is assumed that the Fe in the outermost layer is partially covered by O. Removal of this O or a change in structure causes the Fe to be more exposed and thus the Fe LEIS signal to increase. Offsets have to be taken into account, as in all Fe sputter profiles the Fe signals do not go to zero at high sputter dose. This may be caused by ion beam mixing effects. The results of these simulations are included in Figure 5a (solid curves).

From the simulations of the (Y, Zr) sputter profiles a sputter yield of 0.11 ± 0.05 is obtained. The sputter yield can also be determined from the slope of the Fe sputter profiles at zero sputter dose according to the following relation:

$$\left[\frac{\partial\theta(d)}{\partial d}\right]_{d=0} = -\frac{\theta(0)}{n_0}(\mathrm{SY}) \qquad (2)$$

where $\theta(d)$ is the surface coverage at dose d, n_0 is the maximum Fe density, and SY is the sputter yield. The relation may only be used for those sputter profiles where the Fe_2O_3 is restricted to one layer at most, which is the case up to three ALD cycles. The average sputter yield is determined to be 0.11, assuming that the maximum Fe density is $(2.5 \pm 0.6) \times 10^{15}$ Fe/cm^2.

3.3. Growth Mechanism. *3.3.1. Reaction Pathway*. The two most common ways of metal acetylacetonate precursors to react with oxidic surfaces is by hydrogen bonding and by ligand exchange.[13] In both cases, surface hydroxyls are involved. The OH groups, however, have been removed from our sample surfaces before each ALD experiment. First, the sample surface is cleaned after insertion into the pretreatment chamber (section 2.2.1). The absence of OH groups after the cleaning procedure is confirmed by sputter profiles measured on freshly cleaned 10YSZ samples with LEIS (3 keV $^4He^+$ incident ions), which show that the (Y, Zr) and O signals remain constant for low applied sputter doses ($<5 \times 10^{15}$ $^4He^+$ ions/cm^2).[24] Second, after $Fe(acac)_3$ deposition and before the next ALD cycle the sample is oxidized (section 2.2.1). In a separate experiment it has been checked that the removal of the organic ligands by oxidation only or by a combination of annealing (at 300 °C in ultrahigh vacuum) and oxidation is equally efficient. Furthermore, a second oxidation treatment does not result in a change in the LEIS spectra, nor does it change the $Fe(acac)_3$ adsorption content in the following ALD cycle. However, after oxidation the sample has to be transferred to the ALD reaction chamber. Although this happens in a vacuum of 10^{-7} mbar, it does not guarantee the absence of OH groups before the ALD experiment is begun.

To determine the reaction mechanism of $Fe(acac)_3$ with the 10YSZ surface, a spectroscopic study on liquid- and gas-phase reactions of $Fe(acac)_3$ with a ZrO_2 surface has been carried out.[30] From this study it follows that the reaction of $Fe(acac)_3$ with the ZrO_2 surface can proceed via coordinatively unsaturated Zr sites (cus's). The reaction scheme indicated in ref 30, adapted to our experimental conditions, is depicted in Figure 8. $Fe(acac)_3$ loses two of its three ligands to the surface in the reaction. The loss of one or two ligands is common for metals with 3+ valence; it makes close approach and thereby the reaction of the metal ion with the surface possible. $Fe(acac)_3$ is known to be a very unstable complex, which loses its ligands readily.[22] The third ligand remains weakly attached to the Fe ion. Short exposure to air already causes a removal of the ligand, most likely in the form of Hacac. In the oxidation step of the ALD cycle the atomic oxygen will remove the organic ligands in the form of carbon dioxide and water. The OH group, attached to the Fe ion, is drawn in Figure 8 in analogy with the results described in ref 30, where the infrared photoacoustic spectra clearly show the presence of an Fe−OH band. In that study the OH group is caused by the hydrolysis of the highly unstable remaining Fe−acac function by ambient water, during the sample transfer to the analysis cell. In our case the OH group can only appear on the surface after readsorption of one of the reaction products created in the oxidation reaction involving the acac ligands. Decomposition of the acac ligands will produce significant amounts of water and CO_2. The presence of an OH group on top of an Fe ion will explain the rather slow increase in Fe yield, when the surface is sputtered (Figure 5a). Normally a more rapid increase is observed, when H as the only contaminant is removed from the surface. A different bonding of Fe with the surface, e.g., $Fe-(O-Zr)_3$, is therefore not unlikely.

The Fe load found in the spectroscopic study[30] using electron microprobe analysis (EMA) after $Fe(acac)_3$ deposition equals 2.3×10^{14} Fe ions/cm^2. Van Ommen et al.[19] found values between 8×10^{13} and 3.5×10^{14} Fe ions/cm^2 on ZrO_2 after liquid impregnation. The cross-sectional area of $M(acac)_2$ (with M = Cu or V) equals about 60 Å^2,[13,18] which results in a surface density of 1.7×10^{14} ions/cm^2. The used 10YSZ has a fluorite structure. The highest Zr density is obtained for the (111) surface and equals about 1.1×10^{15} ions/cm^2, obtaining a surface density of 2.8×10^{14} Fe ions/cm^2, when four Zr ions are required for the adsorption of one $Fe(acac)_3$ molecule. This means the Fe load found with EMA[30] agrees with values found in the literature and with estimations made on theoretical grounds. It should also be equal to the 8% Fe_2O_3 surface coverage after one ALD cycle found in this work. From these values a maximum surface density of 2.9×10^{15} Fe ions/cm^2 can be calculated, which is in agreement with the value found from the model used in section 3.2.3.

3.3.2. DRIFT Measurements. The spectroscopic study, mentioned in section 3.3.1,[30] has been extended to $Fe(acac)_3$ on 8YSZ and Fe_2O_3. Figure 9 shows the DRIFT spectra of pure $Fe(acac)_3$, pure $Zr(acac)_4$ and 8YSZ and Fe_2O_3 that have reacted with $Fe(acac)_3$.

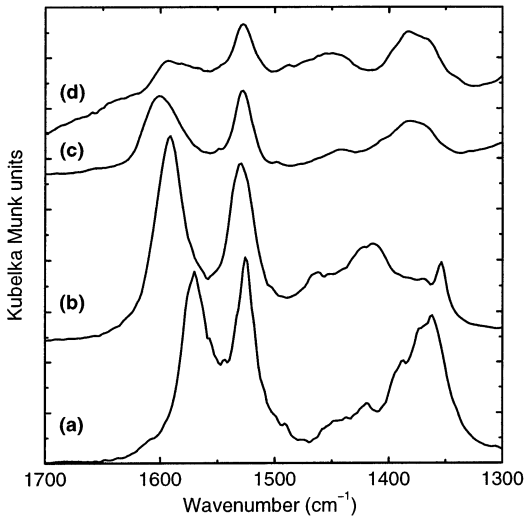

Figure 9. DRIFT spectra of (a) pure $Fe(acac)_3$, (b) pure $Zr(acac)_4$, (c) 8YSZ after reaction with $Fe(acac)_3$, and (d) Fe_2O_3 after reaction with $Fe(acac)_3$. Reactions were carried out in the liquid phase at room temperature.

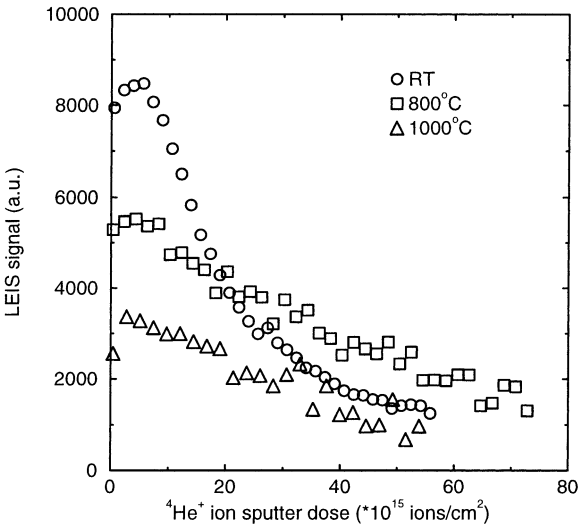

Figure 10. Sputter profiles of Fe after oxidation at 800 and 1000 °C for 5 h in O_2. Before oxidation 10 ALD cycles are deposited onto the sample surface. For comparison the sputter profile after 10 ALD cycles without further oxidation is also given. The increase in the Fe signal at low dose in this sputter profile is caused by structural effects as described in section 3.2.2.

It has been known for quite some time that the positions of the C−O and C−C vibrational modes of the acac licands are influenced by the central metal ion, as decribed by the ligand field theory.[42−44] Inspection of the position of the $\nu_s(C-O)_{ring}$ in spectra a and b shows that this band is situated at 1570 cm^{-1} for $Fe(acac)_3$ and at 1590 cm^{-1} for $Zr(acac)_4$. The $\nu_{as}(C-C-C)_{ring}$ is positioned at 1530 cm^{-1} for both complexes. The $\nu_s(C-O)_{ring}$ vibration is therefore an excellent diagnostic tool to gain information on the nature of the central metal ion.

Spectrum c in Figure 9 shows the 8YSZ support, reacted with $Fe(acac)_3$ in the liquid phase. The $\nu_s(C-O)_{ring}$ vibration is positioned at 1600 cm^{-1}—a slightly higher value than for $Zr(acac)_4$—which is probably due to a contribution of Y−acac surface species. The theoretical assignment of the $\nu_s(C-O)_{ring}$ vibration of $Y(acac)_3$ is at 1610 cm^{-1}.[42] The band at 1600 cm^{-1} in spectrum c is a superposition of Y−acac and Zr−acac contributions. Comparison of spectra c and a makes it perfectly clear, however, that no contribution of Fe−acac surface species is present in spectrum c, which corroborates the reaction mechanism presented in Figure 8. Two Fe−acac bonds are broken upon reaction of $Fe(acac)_3$ with the YSZ surface, and the acac ligands are bonded to the Zr (or Y) coordinatively unsaturated sites. The third ligand is lost due to transport through air (see section 3.3.1).

A relevant question is whether a reaction of $Fe(acac)_3$ with Fe_2O_3 is possible. This experiment was performed, and the DRIFT spectrum is shown in Figure 9 as spectrum d. Weak but distinct bands, attributed to acac surface species, can be observed. Especially the $\nu_{as}(C-C-C)_{ring}$ vibration is clearly present. This indicates that this reaction is indeed possible and confirms the possibility of pyramid-like growth of Fe_2O_3 on YSZ, which was concluded from the sputter profiles.

3.4. Stability of the Fe_2O_3 Overlayer. The sputter profiles of Fe after oxidation at 800 and 1000 °C are given in Figure 10. For comparison the sputter profile measured after 10 ALD cycles without such a high-temperature oxidation is also given. The oxidation clearly causes a decrease in the Fe signal measured in the first LEIS spectra and causes a more gradual decrease of that Fe signal with sputter dose, compared to the result at RT. The decrease of the LEIS signal can be converted to a decrease in surface coverage using the results of Figure 3. After oxidation to 800 and 1000 °C the surface Fe_2O_3 coverages are about 28% and 16%, respectively, while before oxidation the coverage is about 40%. It is unlikely that the iron oxide has evaporated. The gradual decrease of the Fe signal thus indicates that the lower surface coverages are caused by the diffusion of Fe (or iron oxide) into the bulk.

The diffusion coefficient for Fe (iron oxide) diffusion in YSZ at 800 °C is estimated to be on the order of 10^{-23} m^2/s using Fick's diffusion laws,[45] which is 2 orders of magnitude lower than the value found by Van Hassel and Burggraaf.[46] The discrepancy can be attributed at least partly to the experimental starting conditions. Van Hassel et al. used ion implantation to modify the YSZ sample with Fe. The damage caused by this technique provides faster diffusion pathways. Iltis et al.[47] found a diffusion coefficient of 10^{-19} m^2/s for diffusion of Fe in ZrO_2 at 400 °C. This high value would cause such a severe migration of Fe into the bulk that the surface concentration would become too low to be detected in our experiment. The lower diffusion coefficient found in this work compared to those reported in the literature may also indicate the presence of a diffusion barrier layer. Indications for a surface region with a diffusion coefficient lower than that of the bulk were already found in earlier experiments performed by us to determine the self-diffusion coefficient of oxygen in YSZ.

4. Conclusions

$Fe(acac)_3$ readily reacts with YSZ. Saturation of the reaction is achieved at room temperature within 2 min. Consecutive ALD growth cycles increase the Fe_2O_3 coverage by an average value per cycle of 5% of the free YSZ surface. The Fe_2O_3 growth is not restricted to a single monolayer. The maximum Fe surface density equals 2.9×10^{15} particles/cm^2. The sputter yield of Fe (iron oxide) on YSZ with 3 keV $^4He^+$ ions is 0.11 Fe atom/ion. The Fe_2O_3 layer is stable up to 500 °C. For higher temperatures the Fe (iron oxide) dissolves into the bulk. The diffusion coefficient of Fe in YSZ at 800 °C is determined to be 10^{-23} m^2/s.

References and Notes

(1) Suntola, T. *Mater. Sci. Rep.* **1989**, *4*, 261.
(2) Suntola, T. *Thin Solid Films* **1992**, *216*, 84.

(3) Suntola, T. In *Handbook of crystal growth*; Hurle D. T. J., Ed.; Elsevier: Amsterdam, 1994; Vol. 3.
(4) Lakomaa, E.-L. *Appl. Surf. Sci.* **1994**, *75*, 185.
(5) Haukka, S.; Lakomaa, E.-L.; Suntola, T. *Stud. Surf. Sci. Catal.* **1998**, *120*, 715.
(6) Haukka, S.; Lakomaa, E.-L.; Suntola, T. *Appl. Surf. Sci.* **1994**, *82/83*, 548.
(7) Steele, B. C. H. *Solid State Ionics* **1995**, *75*, 157.
(8) Steele, B. C. H. *Mater. Sci. Eng.* **1992**, *B13*, 79.
(9) Bouwmeester, H. J. M.; Kruidhof, H.; Burggraaf, A. J. *Solid State Ionics* **1994**, *72*, 185.
(10) Vervoort, A. G. J.; Scanlon, P. J.; De Ridder, M.; Van Welzenis, R. G.; Brongersma, H. H. *Nucl. Instrum. Methods* **2002**, *B190*, 813.
(11) Van Hassel, B. A.; Burggraaf, A. J. *Appl. Phys.* **1991**, *A53*, 155.
(12) Sasaki, K.; Maier, J. *Solid State Ionics* **2002**, *134*, 303.
(13) White, M. G. *Catal. Today* **1993**, *18*, 73.
(14) Van Der Voort, P.; Mitchell, M. B.; Vansant, E. F.; White, M. G. *Interface Sci.* **1997**, *5*, 169.
(15) Iball, J.; Morgan, C. H. *Acta Crystallogr.* **1967**, *23*, 239.
(16) Roof, R. B. *Acta Crystallogr.* **1956**, *9*, 781.
(17) Kabak, M.; Elmali, A.; Ozbey, S.; Atakol, O.; Kenar, A. *Z. Kristallogr.* **1996**, *211*, 831.
(18) Kenvin, J. C.; White, M. G.; Mitchell, M. B. *Langmuir* **1991**, *7*, 1198.
(19) Van Ommen, J. G.; Hoving, K.; Bosch, H.; Hengstum, A. J.; Gellings, P. J. *Z. Phys. Chem.* **1983**, *134*, 99.
(20) Jacobs, J.-P.; Lindfors, L. D.; Reintjes, J. G.; Jylhä, O.; Brongersma, H. H. *Catal. Lett.* **1994**, *25*, 315.
(21) Van Welzenis, R. G.; Bink, R. A. M.; Brongersma, H. H. *Appl. Surf. Sci.* **1996**, *107*, 255.
(22) Von Hoene, J.; Charles, R. G.; Hickam, M. K. *J. Phys. Chem.* **1958**, *62*, 1098.
(23) Anantharaman, M. R.; Shewale, S. S.; Rao, V.; Seshan, K.; Keer, H. V. *Ind. J. Chem.* **1982**, *A21*, 714.
(24) De Ridder, M.; Van Welzenis, R. G.; Brongersma, H. H. *Surf. Interface Anal.* **2002**, *33*, 309.
(25) Van Der Voort, P.; Babitch, I. V.; Grobet, P. J.; Verberckmoes, A. A.; Vansant, E. F. *J. Chem. Soc., Faraday Trans.* **1992**, *92*, 3635.
(26) Baltes, M.; Colart, O.; Van Der Voort, P.; Vansant, E. F. *Langmuir* **1999**, *15*, 5841.
(27) Brongersma, H. H.; Hazewindus, N.; Van Nieuwland, J. M.; Otten, A. M. M.; Smets, A. J. *Rev. Sci. Instrum.* **1978**, *49*, 707.
(28) Jacobs, J.-P. Ph.D. Thesis, Eindhoven University of Technology, Einhoven, The Netherlands, 1995.
(29) Hellings, G. J. H.; Ottenvanger, H.; Boelens, C. L. C.; Knibbeler, M.; Brongersma, H. H. *Surf. Sci.* **1985**, *162*, 913.
(30) Van Der Voort, P.; Van Welzenis, R. G.; De Ridder, M.; Brongersma, H. H.; Baltes, M.; Mathieu, M.; Van de Ven, P. C.; Vansant, E. F. *Langmuir* **2002**, *18*, 4420.
(31) Wagner, C. D.; Riggs, W. M.; Davis, L. E.; Moulder, J. F.; Muilenberg, G. E. *Handbook of X-ray Photoelectron Spectroscopy*; Perkin-Elmer Corp.: Minnesota, 1979.
(32) Matsunami, N.; Yamamura, Y.; Itikawa, Y.; Itoh, N.; Kazumata, Y.; Miyagawa, S.; Morita, K.; Shimizu, R.; Tawara, H. *At. Data Nucl. Data Tables* **1984**, *31*, 1.
(33) Bohdansky, J.; Roth, J.; Bay, H. L. *J. Appl. Phys.* **1980**, *51*, 2861.
(34) Nenadovic, T.; Perraillon, B.; Bogdanov, Z.; Djordjevic, Z.; Milic, M. *Nucl. Instrum. Methods* **1990**, *B48*, 538.
(35) Betz, G.; Wehner, G. K. In *Sputtering by particle bombardment II*; Behrisch, R., Ed.; Springer-Verlag: Berlin, 1983.
(36) Mitchell, D. F.; Sproule, G. I.; Graham, M. J. *Surf. Interface Anal.* **1990**, *15*, 487.
(37) Brongersma, H. H.; Beirens, L. C. M.; Van der Ligt, G. C. J. In *Material characterisation using ion beams*; Thomas, J. P., Cachard, A., Eds.; Plenum Press: London, 1978.
(38) Cornell, R. M.; Schwertmann, U. *The Iron Oxides: Structure, properties reaction occurrence and uses*; VCH: Weinheim, Germany, 1996.
(39) Jacobs, J.-P.; Maltha, A.; Reintjes, J. G. H.; Drimal, J.; Ponec, V.; Brongersma, H. H. *J. Catal.* **1994**, *147*, 294.
(40) Knözinger, H.; Ratsanamy, P. *Catal. Rev. Sci. Eng.* **1978**, *17*, 31.
(41) Van Leerdam, G. C. Ph.D. Thesis, Eindhoven University of Technology, Eindhoven, The Netherlands, 1991.
(42) Lawson, K. E. *Spectrochim. Acta* **1961**, *17*, 248.
(43) Mikami, M.; Nakagawa, I.; Shimanouchi, T. *Spectrochim. Acta* **1967**, *23A*, 1037.
(44) Nakamoto, K.; McCarthy, P. J.; Martell, A. E. *J. Am. Chem. Soc.* **1961**, *83*, 1272.
(45) Crank, J. *The mathematics of diffusion*, 2nd ed.; Clarendon Press: Oxford, 1957.
(46) Van Hassel, B. A.; Burggraaf, A. J. *Appl. Phys.* **1991**, *A53*, 155.
(47) Iltis, X.; Lefebvre, F.; Lemaignan, C. *J. Nucl. Mater.* **1995**, *224*, 121.